The Oscillating Manometer: A Review of Experimental, Theoretical, and Computational Results

JOHN C. BIERY

Los Alamos Scientific Laboratory, Los Alamos, New Mexico

In a previous paper (*15*) P. D. Richardson raised questions about the numerical and experimental techniques used by the present author in the analysis of the oscillating manometer (*13, 14*). Therefore, a complete review of the experimental and theoretical efforts, to understand fully the problems in measuring and describing fluid behavior in a manometer, is thought advisable. In the following sections the numerical techniques used by the author are reviewed along with a comparison of analytical results of other authors. Also, the secondary effects such as reversal end effects and start-up phenomena in reference to the experimental results are discussed.

VARIATION OF DAMPING FACTOR WITHIN A RUN

Richardson suggested that the damping factor should vary with each half cycle because the initial flat velocity profile is not repeated. The numerical calculations showed this condition to be true (*13, 14*), and the calculated damping factor did vary with each half cycle. The calculated data for run 20 indicate the general effect observed for Newtonian fluids.

Cycle	Damping Factor	
½	0.0281	
1	0.0315	
1½	0.0297	
2	0.0308	avg. = 0.303
2½	0.0301	
3	0.0305	
asymptotic value	0.303	

Thus, the damping factor fluctuated and finally converged after 4 to 5 cycles to an asymptotic value. In the comparisons made between computed and experimental damping factors, the values used were these asymptotic values or an overall average of all half cycle damping factors after the first full cycle.

ACCURACY OF THE NUMERICAL METHODS

The accuracy of the numerical integration technique is of prime interest because of the question of the secondary effects and because of the general conclusion drawn in the previous two papers. Because of the importance of accuracy, much effort was expended in determining the effects of grid size (Δr^*, Δt^*) reduction upon the computational results. The numerical technique as previously described (*13, 14*) involved determining velocity profiles from the equation of motion, integrating the profile over the radius to find an average velocity, and then determining the movement of the column of liquid with this average velocity over the time increment, Δt^*. A forward difference form of the differential equation of motion was used in the first integration to obtain the velocity profile. And, as indicated by Douglas (*10*), the results from this form of integration of a parabolic differential equation can be expected to converge to the exact solution if R, the coefficient of the divided difference representing the second derivative with respect to distance, is non-negative and less than or equal to ½. In the heat equation used in the example by Douglas the coefficient is $\Delta t/(\Delta x)^2$. For the manometer problem the coefficient is

$$\frac{\Delta t^*}{6\Omega_1(\Delta r^*)^2}$$

With this requirement met, the maximum difference between the computed and exact result, $\max |v^* - v^*_{cal}| \leq B[(\Delta r^*)^2 + \Delta t^*]$ as indicated by the theorem on page 6 of reference *10*. The coefficient B depends upon the upper bounds of v^*_{tt} and v^*_{rrrr} and upon the size of total time interval being investigated. Therefore, as Δt^* and Δr^* tend toward zero, the numerical solution converges toward the exact solution of the differential equation. There is no requirement that the factor R remain at a constant value as Δt^* and Δr^* change but that R be non-negative and be less than or equal to ½.

The total problem is one of solving an integro-differential equation. The actual convergence criteria required for the general equation have not been fully investigated. However, in the opinion of Douglas, if a properly convergent difference analog is used and the quadrature method has equal accuracy, the overall integration will also converge as Δt^* and Δr^* are made sufficiently small.

In an actual problem the convergence properties of the solution can be investigated by observing the changes in the final result as the grid size is refined. The procedure used in the manometer integration was to find a Δt^* for a given Δr^* where the solution was stable and then reduce Δt^* and Δr^* with this constant ratio of $\Delta t^*/\Delta r^*$. One example of this procedure is given in Table 1.

Table 1. Variation of Damping Factor with Varying Δt^* for Run 14 with $\Delta r^* = 0.1$

Δt^*	0.20		0.10		0.05		0.025
ζ	0.1948		0.1978		0.1990		0.1994
$\Delta\zeta$		0.0030		0.0012		0.0004	

In this example, ζ, the damping factor, converged to a value of 0.1996 quite rapidly and was within 0.3% of this value with $\Delta t^* = 0.05$. Thereafter, for almost all integrations, the ratio $\Delta t^*/\Delta r^*$ was maintained constant at ½, and the convergence of the problem was observed as the sizes of Δt^* and Δr^* were reduced successively by factors of 2. The only danger in this procedure is that R may become greater than ½ as the grid is refined. However, when ½ is substituted for $\Delta t^*/\Delta r^*$ in R, the requirement on Δr^* is that it be greater than $1/6\Omega_1$. The range of Ω_1 for all runs was from 8 to 959. The larger Ω_1, the smaller a grid was required to obtain good convergence of ζ, the damping factor. With $\Omega_1 = 959$, Δr^* could be reduced to 0.000175 before the ½ level was exceeded by

Table 2. Convergence of Damping Factors with Grid Refinement with $\Delta t^*/\Delta r^* = ½$

Run No.	Ω_1	Δr^*	ζ	Ratio $\frac{\Delta\zeta_n}{\Delta\zeta_{n+1}}$		% Error in ζ
20	959	0.10	0.01552			40.8
				0.00720		
		0.05	0.02272		3.09	13.3
				0.002330		
		0.025	0.02505		3.03	4.4
				0.000770		
		0.0125	0.02582			1.4
estimated convergence			0.026196			
21		0.10	0.0553			9.93
				0.00420		
		0.05	0.0595		3.23	3.07
		0.025	0.0608	0.0013		0.945
estimated convergence			0.006138			

R. With $\Omega_1 = 8$, Δr^* must be kept above 0.02. In all cases convergence was reached before the grid size was reduced to these levels.

Many calculations were run with changes in grid size as indicated above. In all cases the change in damping factor, $\Delta\zeta$, with a halving of the grid was approximately one-third of the size of $\Delta\zeta$ for the previous halving of the grid. Examples of this variation are shown in Table 2.

With $\Delta t^*/\Delta r^*$ set at a constant factor of ½, the product $\Omega_1 \Delta r^*$ determines the size of the coefficient group R. From all of the convergent data, this product was found to have a nearly constant value of 1 when the damping factor had approached to within 0.1% of the convergent value. Thus, for this particular problem convergence was satisfactorily complete when R equaled 1/6 and $\Delta t^*/\Delta r^*$ equaled ½.

FLOW REVERSAL END EFFECT

The data presented above indicate that the numerical procedure converged in all cases and the criteria for convergence was satisfied in all instances. Thus, the numerical solution can be used as a basis for comparing physical data and to indicate whether or not other effects are operative in the manometer behavior. When this comparison was made with the work previously reported (*13, 14*), deviations from this base were found. These deviations might be due to turbulence, effects of curvature, or end effects of the flow reversal, surface tension, and falling films. The effects of turbulence and curvature were studied separately and, as reported in (*13*) were found to be negligible for most of the experimental situations. [However, Richardson (*15*) has indicated that in unsteady flow the curvature effect may be greater than that found in steady flow.] The reversal end effect had been observed experimentally by watching the flow of particles in the fluid as it flowed up the center and toward the edge of the tube across the meniscus surface. [Note: In the work of Valensi and Clarion (*6, 8*) much effort was expended to observe flow patterns in the manometer fluid as it was oscillating. However, the technique used only observed the behavior of the fluid at the ends of the column, and therefore, the results they report really indicated the types of flow patterns that could be expected in this region. Their photographs indicate that the flow varied from a smooth reversal to one in which eddies of fluid were noted. In extreme cases, turbulence in the end flow was found. These effects were similar to those observed by the author when particles were added to the liquid to indicate the flow pattern.] Therefore, all deviations between the experimental data and the calculational data were ascribed to the end effect since the surface tension and falling film effects were also found to be minor for most of the fluids studied. However, if Richardson's statement about additional viscous dissipation due to unsteady flow in a curved tube is correct, the additional term then accounts for all secondary effects involving viscosity and the constant should be named K(secondary). After postulating a form of the viscous dissipation in the end flow, the data indicated that for the three diameter tubes studied and the various liquids investigated that the end effect took a form $F_T = K_{\text{end}}\, S <v_z> \mu$ with K_{end} as an apparent constant.

ACCURACY OF EXPERIMENTAL DATA

The value of K_{end} as presented certainly is dependent upon the accuracy of the experimental data in addition to the accuracy of the numerical calculations. A fairly complete tabulation of the statistical analysis of the damping factor calculations is given elsewhere (*13*). That analysis can be interpreted in two ways, one, as a comparison of the simulation results to the experimental results, and two, as a statistical analysis of the experimental data since the first two sets of data agree to within an error of + 0.82%. Each cycle damping factor was within ± 11% of the average value for the total run and the standard deviation of each cycle measurement was 3.8%. The standard deviation of the mean values was 0.69%. These statistical values indicate that the 95% confidence band lies within ± 1.8% of the average values. Since the simulation damping factor results without the end effect inclusion were 10 to 15% low for the 1.25 cm. tube, 10% for the 1.06 cm. tube, and 5% for the 0.456 cm. tube, the raw numerical simulation data and the experimental data were statistically significantly different, and therefore, some added effect must be considered.

CORRELATION OF CALCULATIONAL DATA WITH VALENSI NUMBER

One method of testing the continuity of the manometer calculation results is to plot calculated damping factors vs. a manometer similitude number, $r^2\omega_p/\nu$, as proposed by Valensi (*2*) and Ury (*11*). [Note: Since this number was first proposed by Valensi, the author would like to call it the Valensi Number, N_{Va}. In terms of the dimensionless groups of the author (*13*), the Valensi number is equal to $\sqrt{48}\ \Omega_1/L^{*1/2}$. The damping factor as used by the author (*13, 14*) and Ury is the same as the λ/ω_p used by Valensi (*2, 3*).]To check carefully the calculational results, the damping factors, ζ, from the calculations with no end effect correction, were plotted vs. N_{Va}. Figure 1 shows the results of that plot. The calculational points were found to fall on a smooth continuous curve. However, the curve does not exactly correspond in any section to the modified correlation equations proposed by Valensi (*2, 7*). This result should be expected since the equations as proposed and developed were for two simplified cases, one for a fully developed profile and one for a boundary-layer condition.

CORRELATION OF EXPERIMENTAL DATA WITH VALENSI NUMBER: SECONDARY EFFECTS

Secondary effects are probably responsible for increasing damping of from 1 to 10% in all of the manometer data so far reported in the literature. All of Menneret's data as presented by Valensi (*3*) and Mennert (*1*) and the experimental data of the author are plotted on Figure 1. In all cases, the experimental data fall either on the calculational curve or up to 15% above the curve. This positioning of the data would indicate that secondary effects increased the observed damping factors over those expected from the primary fluid flow patterns.

FIRST CYCLE EFFECTS

In these data of the author, the damping factor of the first oscillation was usually not included in the overall average since it was generally high. A tabulation of these first cycle results are shown in Table 3.

Table 3. First Cycle Damping Factors as Compared to the Average of the Run

N_{Va}	Radius (cm.)	Size of 1st Cycle— % Above Average	K	$K_{\text{avg.}}$
775	1.251	+ 4.4%	0.26	
167	1.251	+ 2.5%	0.32	
572	1.052	+ 7.5%	0.35	0.30
107	0.4545	+19.2%	0.30	
22.7	0.4545	+ 7.8%	0.27	

These data show that the first cycle was from 2.5 to 19% high. For the runs not shown, the first cycle gave values very near the average. The effect does not correlate well with N_{Va} but is a strong function of r. The error becomes greater as N_{Va} increases for a given r and as r decreases for a constant N_{Va}. An empirical function, % error =

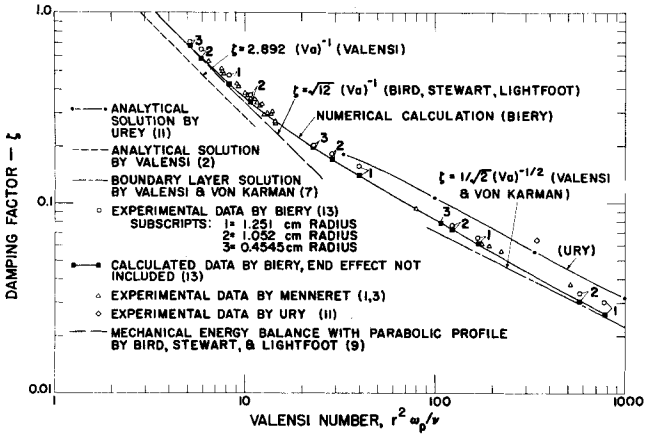

Fig. 1.

$K\ N_{Va}^{1/2}/r^{2.3}$ was fitted to the data with $K = 0.30$. The application of this formula to another experimenter's data is questionable since the method of operating the experiment must influence the effect. However, the effect is real and must be considered.

This increase in damping factor on the first cycle was due to two effects. First, some force must be used to displace the legs of the manometer. This force is exerted by applying air pressure to one leg or vacuum to the other. As the air rushes out from the high pressure side or into the low pressure side, an additional damping force is exerted momentarily by the momentum effects of the high velocity air flow. This effect is discussed in the second manometer paper by the author (*14*). The amount of damping must be a function of the air pressure required and the length of air column.

Second, the first cycle may have added damping from turbulence induced by the relatively high velocity with the initial large leg displacement. Probably this effect manifests itself as vortices at the ends of the fluid columns. The author noted the rotating vortices for water in the 1.256 cm. radius manometer. Also, similar effects were photographed by Clarion and Valensi (*6, 8*).

This last effect has been roughly characterized by the dimensionless group, $h^2\omega_p/\nu$. The author in reviewing his experimental data found the values of the group where turbulence at the ends of the tube was suspected varied from 50,800 for run 20 with $N_{Va} = 775$ to 53,600 for run 31 with $N_{Va} = 570$. No turbulence was found with numbers below 34,000. These results agree somewhat with Richardson's (*12*) observation that the transition is near 46,000 with $N_{Va} = 500$.

In all cases Menneret's data lay slightly above the calculated curve as shown in Figure 1. And significantly, all of these data were obtained on the first full cycle of oscillation (*1*). As indicated above, this cycle is the poorest one to use because of the start-up effects. Thus, some of the increase in damping factor might be due to these initial effects. The influence of air flow might have been particularly accentuated since the radii of the tubes used ranged from 0.1 to 0.56 cm. This start-up effect may be the reason that Menneret found the damping to vary as a function of initial leg height differential. Turbulence should not have been an important factor in this case since $h^2\omega_p/\nu$ was quite small for most of the runs.

REVERSAL FLOW END EFFECT

Secondary Viscous Dissipation Effects

The reversal flow end effect and other secondary dissipation effects were also present in Menneret's data but the effects were very small. The dimensionless group, $\Phi = \frac{1}{8}\, r^2 K_{end} L$, gives an indication of the size of the effect to the viscous damping effects. The damping factor as calculated by the calculational technique should be increased by a factor of $(1 + \Phi^{-m})$ where m is the slope of the ζ vs. N_{Va} curve at the appropriate value of N_{Va}. The values of Φ were calculated for Menneret's data, and the corrections were found to range from 0.1 to 2.1% for the data near $N_{Va} = 10$ and from 0.8 to 2.2% for the data with N_{Va} between 100 and 500.

THEORETICAL RESULTS OF PREVIOUS INVESTIGATORS

Before a conclusion is reached about the usefulness of the numerically calculated data, the various manometer equations and correlations should be examined in light of the accumulated data, both experimental and calculated. The first theoretical calculation of manometer response was made by Valensi (*2*). His result was reported by Richardson and is repeated here in Equation (1).

$$\zeta = 2.892\ (N_{Va})^{-1} \qquad (1)$$

The velocity equation that Valensi derived indicated that the velocity profile should be a J_o Bessel function of the radius with a cosine time variable amplitude. Equation (1) is plotted on Figure 1. Obviously, the assumptions that were included in the derivation were too incomplete to describe adequately the physical system. However, this relationship was used to correlate Menneret's data and the coefficient was arbitrarily adjusted to 3.9536 in a later article (*3*). The incompleteness of the solution was recognized. Therefore, Valensi and Vogel (*5*) presented a more complete solution which included an infinite series of J_o Bessel functions for the radial velocity dependence. However, when this solution was simplified to obtain an asymptotic solution near critical damping, the same dependence shown in Equation (1) resulted.

In 1948 Valensi and Von Karman (*7*) applied the boundary-layer theory to obtain an asymptotic solution for very small damping factors. They assumed that the fluid remained stationary and the tube moved with a cosine motion. They were able to solve the equation of motion with the simplifying assumptions of the boundary-layer approach. The result is shown as

$$\zeta = \frac{1}{\sqrt{2}}\ (N_{Va})^{-1/2} \qquad (2)$$

This equation is plotted in Figure 1 and is found to agree very well with the numerical simulation results as N_{Va} approaches 1,000. Valensi, however, readjusted the coefficient to 0.82 to agree with Menneret's data.

A new attack on the manometer problem was made by Ury (*11*) in 1962. In this case, a solution was obtained for two coupled differential equations, the standard second-order damped harmonic differential equation and the Navier-Stokes equation. In this approach the mass of the manometer fluid was readjusted by a factor, δ. The values of δ and ζ were obtained from the general solution which took two equivalent forms, one where the radial dependence was given by an infinite series of J_o Bessel functions and the other by a J_o and J_1 Bessel functions of complex arguments. The equations were solved approximately for N_{Va} numbers between 100 and 1,000. These results are plotted on Figure 1. The slope is approximately $-\frac{1}{2}$ but the values are significantly above the experimental results of the author and Menneret and the calculational results of the author and Van Karman and Valensi.

An interesting anomaly is that the data shown in Figure 5 of Ury's article for mercury in a plastic tube manometer gives a damping factor for the middle of the curve of 0.0639 with $N_{Va} = 337$. As seen in Figure 1, this value does not correspond to the other data but does somewhat agree with Ury's curve. Large secondary effects probably have increased the damping factor. If the plastic tube was flexible, then possibly added dissipation could occur

in the movement of the tube itself.

Finally, Bird, Stewart, and Lightfoot presented in their book (9) a solution for the manometer problem in which they utilized the mechanical energy balance along with an assumed time varying parabolic velocity profile. When their differential equation is converted in terms of the damping factor and the Valensi number, the following equation results.

$$\zeta = \sqrt{12}\ (N_{Va})^{-1} \qquad (3)$$

The slope is the same as given by Valensi, but the coefficient is significantly larger. The equation is plotted on Figure 1. The agreement with the calculated results of the author is very good for conditions near critical damping. Equation (3) appears to be a good asymptotic solution near critical damping.

The use of a parabolic profile near critical damping is a logical choice since it is found in steady state laminar flow of Newtonian fluids in circular pipes. Also, the calculated velocity profiles of the author (*13*) did approach parabolic at critical damping.

These results indicate that tthe boundary-layer solution for high N_{Va} numbers and the mechanical energy balance, parabolic profile solution for small N_{Va} numbers give good asymptotic solutions to the manometer problem. Also, the calculated results of the author tend toward these solutions. All experimental data taken so far fall on or above the calculated curves.

CONCLUSIONS

The statistical and experimental techniques that were used to calculate and measure U-tube manometer behavior in two previous publications (*13, 14*) have been reviewed. The numerical techniques were shown to meet the necessary requirements for convergence, and data were presented to show the rate of convergence when the grid size was refined. Also, the statistical analysis of the experimental data was reviewed to show that the 95% confidence interval about the average data was ± 1.8%. Since the difference between the two sets of data, calculated and experimental, was 5 to 15%, other dissipative effects other than those represented in the equation of motion had to be included.

In an attempt to determine the relationship of the calculated results with previously published data, correlation, and derived equations, all of these data along with the calculated data were plotted as a function of the Valensi number. The numerically calculated results were found to agree almost exactly with two asymptotic solutions, one derived from the boundary-layer theory by Von Karman and Valensi and the other derived with the use of the mechanical energy balance and the time varying parabolic profile. All experimental data were found to be on or above these limiting curves. The secondary effects of start-up, reversal end effect, and turbulence were discussed in reference to the experimental data.

Actually, to use the manometer as a viscometer as suggested by Richardson and earlier by Menneret, these secondary effects, particularly the flow reversal end effect and the unsteady flow in a curved tube, should be studied more rigorously by taking more experimental data in large diameter manometers and by actually calculating the flow patterns and the viscous dissipation that can be expected in the flow at the ends of the tube and in the curved position of the tube. With this procedure a more accurate K_{end} constant can be developed or a more rigorous formulation can be postulated to account for the additional viscous dissipation.

ACKNOWLEDGMENT

The author wishes to thank Professor P. D. Richardson for indicating the previous work which was performed experimentally and analytically on the U-tube manometer problem. This work was performed under the auspices of the U. S. Atomic Energy Commission.

NOTATION

B = coefficient of function describing error between exact and calculated results
F_T = force at ends of liquid legs owing to flow reversal, dynes
g = acceleration due to gravity, cm./sec.^{2}
K = arbitrary constant in correlating errors observed in the first cycle of oscillation
K_{end} = constant relating reversal end effect force to velocity, area, and viscosity, cm.$^{-2}$
L = length of fluid column in tube, cm.
m = exponent for Φ in adjusting damping factor for flow reversal end effect
R = coefficient of the divided difference representing the second derivative in the forword difference representation of a parabolic differential equation
S = cross-sectional area of tube, sq.cm.
r = tube radius, cm.
v^* = dimensionless longitudinal velocity in manometer, exact solution to differential equation, $V^* = v\ [3/2\ rg]^{-1/2}$
v^*_{tt} = second partial time derivative of velocity
v^*_{rrrr} = fourth partial radial derivative of velocity
v^*_{cal} = longitudinal velocity in manometer; result calculated from difference equation
$\langle v_z \rangle$ = average fluid velocity in axial direction
N_{Va} = Valensi number $= r^2\omega_p/v$

Greek Letters

Δr^* = numerical integration radial increment
Δt^* = numerical integration time increment
$\Delta t/(\Delta x)^2$ = coefficient, R, in heat Equation finite difference representation
Ω_1 = dimensionless reciprocal kinematic viscosity: $(\rho/\mu)\ (gr_o^3/24)^{1/2}$
ν = kinematic viscosity $= \mu/\rho$, sq.cm./sec.
ρ = density of fluid, g./cc.
Φ = dimensionless group indicating relative effects of flow reversal to viscous damping, $\Phi = \frac{1}{8}\ r^2K_{end}L$
δ = factor for adjusting the mass in the manometer [see (*11*)]
ζ = damping factor in second-order damped harmonic differential equation [see (*13*)]
Δ = log decrement of Richardson
λ/ω_p = damping factor of Valensi $= \zeta$
ω_p = natural oscillation frequency of the systems, $\omega_p = \sqrt{2\ g/L}$
μ = Newtonian viscosity; dyne sec./sq.cm.

LITERATURE CITED

1. Menneret, M. M., *J. Phys. Theor. Appl.*, **I**, 753 (1911).
2. Valensi, Jacques, *Comptes Rendus*, **224**, 446 (1947).
3. ———, and Claire Clarion, *ibid.*, **224**, 532 (1947).
4. ———, *ibid.*, **224**, 813 (1947).
5. ———, and Theodore Vogel, *ibid.*, **224**, 1695 (1947).
6. ———, and Claire Clarion, *ibid.*, **226**, 554 (1948).
7. Von Karman, Theodore and Jacques Valensi, *Comptes Rendus*, **227**, 105 (1948).
8. Valensi, Jacques, Claire Clarion, and Frederick Zerner, *ibid.*, **230**, 2002 (1950).
9. Bird, R. B., W. E. Stewart, and E. N. Lightfoot, "Transport Phenomena" 1st Ed., pp. 229-231, John Wiley, New York (1960).
10. Douglas, J., Jr., *Adv. Computers*, **2**, 1 (1961).
11. Ury, J. F., *Int. J. Mech. Sci.*, **4**, 349 (1962).
12. Richardson, P. D., *ibid.*, **5**, 415 (1963).
13. Biery, J. C., *AIChE J.*, **9**, 606 (1963).
14. *Ibid.*, **10**, 551 (1964).
15. Richardson, P. D., *ibid.*, **13**, 821 (1967).